# Full-Wave Hamiltonian Analysis of a Coaxial-Fed 3D Microwave Cavity Resonator

Soomin Moon and Thomas E. Roth

Elmore Family School of Electrical and Computer Engineering, Purdue University, West Lafayette, IN 47906, USA (rothte@purdue.edu)

Abstract—Quantum electromagnetic effects in superconducting circuits are promising phenomena to develop revolutionary quantum information processing technologies. To design complex circuits, there is a need for the development of accurate full-wave numerical models. In this work, we study the simpler classical full-wave Hamiltonian of a coaxial-fed rectangular waveguide cavity to validate field-based parts of the corresponding quantum Hamiltonian. We present the formulation of the system Hamiltonian and derive equations of motion. We compare results from our formulation using numerical eigenmodes to traditional transmission simulations of the system to validate the approach.

#### I. Introduction

Superconducting circuits that operate at microwave frequencies are one of the most promising quantum information processing architectures [1]. To improve these systems, full-wave quantum numerical models are increasingly of interest [2], [3]. However, validating the accuracy of these models can be difficult due to the complexity of the hardware and the formulations themselves. Here, we study a classical version of the Hamiltonian proposed in [3] to more easily validate the computation of certain field-dependent parameters for the geometry shown in Fig. 1, which is representative of part of a 3D transmon architecture [4].

In this work, we present the formulation of the classical full-wave Hamiltonian applicable to Fig. 1. We then derive equations of motion for this system when driven by impressed currents in the coaxial subdomains. We numerically validate part of this formulation, with further results from the time domain dynamics to be presented at the conference.

#### II. FORMULATION

The method of [3] uses a projector-based approach to decompose the system into subdomains that can be more easily quantized. Each subdomain is terminated with complementary perfect electric conductor (PEC) and perfect magnetic conductor (PMC) boundary conditions at their interfaces (see Fig. 1) so that each subdomain eigenvalue problem is Hermitian. The subdomain dynamics are then tied together through the field profiles at the interfaces. Considering this, we expand the subdomain fields using eigenmodes that are solutions to the wave equation in each subdomain. For cavity fields, we have

$$\mathbf{E}(\mathbf{r},t) = \sum_{k} \sqrt{\frac{\omega_k}{2\epsilon_0}} (a_k(t) + a_k^*(t)) \mathbf{E}_k(\mathbf{r}), \tag{1}$$

$$\mathbf{H}(\mathbf{r},t) = -i\sum_{k} \sqrt{\frac{\omega_k}{2\mu_0}} (a_k(t) - a_k^*(t)) \mathbf{H}_k(\mathbf{r}), \qquad (2)$$

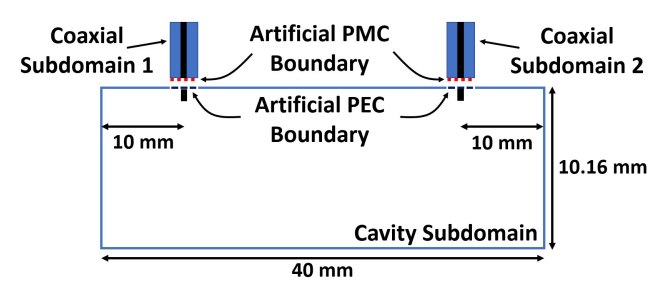


Fig. 1. Schematic illustration of the subdomains for the projector-based full-wave Hamiltonian analysis of a coaxial-fed rectangular waveguide cavity.

where  $\mathbf{E}_k$  and  $\mathbf{H}_k$  are spatial eigenmodes,  $\omega_k$  are the eigenvalues, and  $a_k$  combines the canonical conjugate field amplitudes  $q_k$  and  $p_k$  as  $a_k(t) = \frac{1}{\sqrt{2}}(q_k(t) + ip_k(t))$ . For coaxial fields, there is a continuum of modes so the expansion becomes

$$\mathbf{E}_{p}(\mathbf{r},t) = \sum_{\lambda} \int_{0}^{\infty} \sqrt{\frac{\omega_{\lambda p}}{2\epsilon_{0}}} \times (a_{\lambda p}(t,\omega_{\lambda p}) + a_{\lambda p}^{*}(t,\omega_{\lambda p})) \mathbf{E}_{\lambda p}(\mathbf{r},\omega_{\lambda p}) d\omega_{\lambda p}, \quad (3)$$

where p indexes the port subdomains and  $\lambda$  differentiates between transverse mode profiles with corresponding eigenvalues  $\omega_{\lambda p}$ . The definition of  $a_{\lambda p}(t,\omega_{\lambda p})$  and  $\mathbf{H}_p$  follow the format of the cavity fields, adjusted for the continuum of modes.

These mode expansions may now be substituted into the full projector-based Hamiltonian, which here is

$$H = H_O + H_P + H_{OP} + H_{JP} + H_{MP}, \tag{4}$$

where each Hamiltonian will be defined explicitly shortly. First,  $H_Q(H_P)$  is the cavity (coaxial) subdomain Hamiltonian, which after using the eigenmode orthogonality simplifies to

$$H_Q = \sum_k \omega_k a_k^* a_k,\tag{5}$$

$$H_P = \sum_{p,\lambda} \int_0^\infty \omega_{\lambda p} a_{\lambda p}^*(t,\omega_{\lambda p}) a_{\lambda p}(t,\omega_{\lambda p}) d\omega_{\lambda p}.$$
 (6)

The other Hamiltonians represent interactions between fields in different subdomains and with impressed current sources that drive the system. The cavity-coaxial interaction is

$$(2) H_{QP} = \sum_{k,p,\lambda} \int_0^\infty g_{k,\lambda p}(a_k + a_k^*)(a_{\lambda p} + a_{\lambda p}^*) d\omega_{\lambda p}, (7)$$

$$g_{k,\lambda p} = \iint \frac{c_0}{2} \sqrt{\frac{\omega_{\lambda p}}{\omega_k}} \left[ \mathbf{H}_k \cdot (\mathbf{E}_{\lambda p} \times \hat{n}_p) \right] d\mathbf{r}, \tag{8}$$

where the surface integration occurs over the interface between subdomains and  $\hat{n}_p$  is the unit normal pointing into the cavity. The interaction of impressed currents with TEM coaxial fields (other mode profiles can be considered similarly) are

$$H_{JP} = -i\sum_{p,\lambda} s(t)g_{Jp} \int_0^\infty \frac{1}{\sqrt{\omega_{\lambda p}}} \left(a_{\lambda p} - a_{\lambda p}^*\right) \times \cos\left(\frac{\omega_{\lambda p}}{c} z_{\text{ref}}\right) d\omega_{\lambda p}, \quad (9)$$

$$H_{MP} = -\sum_{p,\lambda} s(t) g_{Mp} \int_0^\infty \frac{1}{\sqrt{\omega_{\lambda p}}} \left( a_{\lambda p} + a_{\lambda p}^* \right) \times \sin\left(\frac{\omega_{\lambda p}}{c} z_{\text{ref}}\right) d\omega_{\lambda p}. \quad (10)$$

Here, s(t) and  $z_{\rm ref}$  are the temporal profile and location of impressed electric and magnetic current densities, and

$$g_{Jp} = \frac{1}{\eta_p} \sqrt{\frac{2\ln(b_p/a_p)}{\epsilon_p c_p}}, \ g_{Mp} = \sqrt{\frac{2\ln(b_p/a_p)}{\mu_p c_p}},$$
 (11)

where  $a_p$  ( $b_p$ ) is the inner (outer) radius of the coaxial line and material properties are those from the coaxial subdomains. By implementing the current sources in this way, they produce an electric field propagating toward the cavity subdomain with an amplitude given by s(t) and no backwards radiation.

With the Hamiltonians appropriately formulated, equations of motion can be derived for the  $a_k$  and  $a_{\lambda p}$ 's by taking their Poisson bracket with H. This results in

$$\frac{\partial a_k}{\partial t} = -i\omega_k a_k - i\sum_{p,\lambda} \int_0^\infty g_{k,\lambda p}(a_{\lambda p} + a_{\lambda p}^*) d\omega_{\lambda p}, \quad (12)$$

$$\frac{\partial a_{\lambda p}}{\partial t} = -i\omega_{\lambda p} a_{\lambda p} - i\sum_{k} g_{k,\lambda p} (a_k + a_k^*) 
+ \frac{s(t)}{\sqrt{\omega_{\lambda p}}} \left[ g_{Jp} \cos\left(\frac{\omega_{\lambda p}}{c} z_{\text{ref}}\right) + ig_{Mp} \sin\left(\frac{\omega_{\lambda p}}{c} z_{\text{ref}}\right) \right].$$
(13)

# III. NUMERICAL RESULTS

The geometry considered for numerically validating this formulation is shown in Fig. 1. The dimension of the cavity is  $22.86 \times 10.16 \times 40 \, \mathrm{mm}^3$ . The coaxial regions have  $a_p = 0.05 \, \mathrm{mm}, \, b_p = 1 \, \mathrm{mm}, \, \epsilon_r = 12.92, \, \mathrm{and} \, \mu_r = 1$ . The length that the inner conductor protrudes into the cavity is varied according to the range shown in Fig. 2.

To begin verifying the accuracy of the Hamiltonian, we numerically find eigenmodes of the cavity region shown in Fig. 1 and use these to compute  $g_{k,\lambda p}$  for the  $\mathrm{TE}_{101}$  mode coupled to the TEM mode of the coaxial regions. From inputoutput theory, the  $g_{k,\lambda p}$  of a single interface can be related to the decay rate of the cavity through that interface as [5]

$$\gamma_p = 2\pi \, g_{k,\lambda p}^2. \tag{14}$$

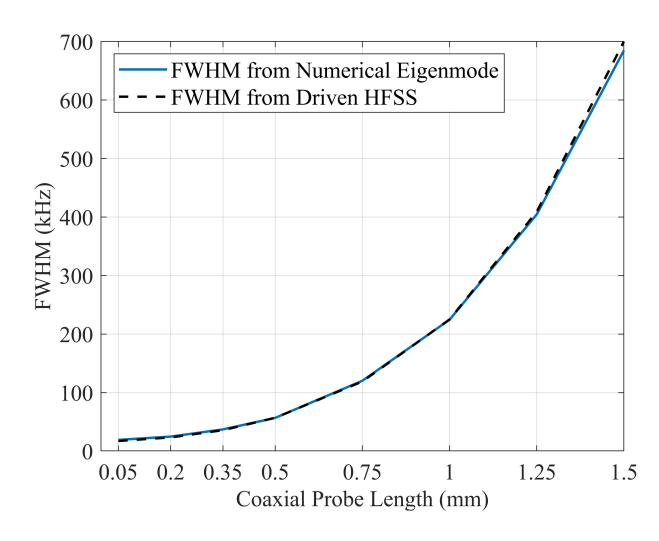


Fig. 2. Comparison of the transmission FWHM when using the formulation of this work and directly computing the transmission with HFSS.

The corresponding full-width half-maximum (FWHM) of the intensity transmission function (i.e.,  $|S_{21}|^2$ ) is then given by  $\sum_p \gamma_p/2\pi$ . The computation of the FWHM via (14) is compared against that found by directly simulating the  $S_{21}$  of the geometry in HFSS in Fig. 2, showing excellent agreement. At the conference, we will also show results of solving the coupled differential equations (12) and (13) to fully validate this Hamiltonian formulation.

#### IV. CONCLUSION

This work presented a full-wave Hamiltonian analysis method for a coaxial-fed 3D microwave cavity using a projector-based approach. This formulation is useful as it can help validate the field-based portions of the quantum full-wave Hamiltonian proposed in [3]. Our future work will include incorporating a small dipole antenna into the cavity to validate the field-qubit coupling Hamiltonian given in [3], as well as solving the full-wave quantum model in its entirety.

## ACKNOWLEDGEMENT

This material is based upon work supported by the National Science Foundation under Grant No. 2202389.

## REFERENCES

- P. Krantz, M. Kjaergaard, F. Yan, T. P. Orlando, S. Gustavsson, and W. D. Oliver, "A quantum engineer's guide to superconducting qubits," *Applied Physics Reviews*, vol. 6, no. 2, p. 021318, 2019.
- [2] Z. K. Minev, Z. Leghtas, S. O. Mundhada, L. Christakis, I. M. Pop, and M. H. Devoret, "Energy-participation quantization of Josephson circuits," npj Quantum Information, vol. 7, no. 1, pp. 1–11, 2021.
- [3] T. E. Roth and W. C. Chew, "Macroscopic circuit quantum electrodynamics: A new look toward developing full-wave numerical models," IEEE Journal on Multiscale and Multiphysics Computational Techniques, vol. 6, pp. 109–124, 2021.
- [4] H. Paik, D. I. Schuster, L. S. Bishop, G. Kirchmair, G. Catelani, A. P. Sears, B. Johnson, M. Reagor, L. Frunzio, L. I. Glazman et al., "Observation of high coherence in Josephson junction qubits measured in a three-dimensional circuit QED architecture," *Physical Review Letters*, vol. 107, no. 24, p. 240501, 2011.
- [5] D. F. Walls and G. J. Milburn, Quantum Optics. Springer Science & Business Media, 2007.